Acta Biomaterialia 64 (2017) 137–147

Contents lists available at ScienceDirect

Acta Biomaterialia

journal homepage: www.elsevier.com/locate/actabiomat

Full length article

Electrospraying of microfluidic encapsulated cells for the fabrication of cell-laden electrospun hybrid tissue constructs

L. Weidenbacher [a,b,c,1], A. Abrishamkar [a,d,1], M. Rottmar [b], A.G. Guex [a,b], K. Maniura-Weber [b], A.J. deMello [d], S.J. Ferguson [c], R.M. Rossi [a], G. Fortunato [a,*]

[a] Empa, Swiss Federal Laboratories for Materials Science and Technology, Laboratory for Biomimetic Membranes and Textiles, St. Gallen, Switzerland
[b] Empa, Swiss Federal Laboratories for Materials Science and Technology, Laboratory for Biointerfaces, St. Gallen, Switzerland
[c] Institute for Biomechanics, Department of Health Sciences and Technology, ETH Zürich, Zürich, Switzerland
[d] Institute for Chemical and Bioengineering, Department of Chemistry and Applied Bioscience, ETH Zürich, Zürich, Switzerland

ARTICLE INFO

Article history:
Received 14 June 2017
Received in revised form 21 September 2017
Accepted 9 October 2017
Available online 10 October 2017

Keywords:
Microfluidic
Cell encapsulation
Tissue engineering
Cytotoxicity
Electrospinning
Cell spraying

ABSTRACT

The fabrication of functional 3D tissues is a major goal in tissue engineering. While electrospinning is a promising technique to manufacture a structure mimicking the extracellular matrix, cell infiltration into electrospun scaffolds remains challenging. The robust and *in situ* delivery of cells into such biomimetic scaffolds would potentially enable the design of tissue engineered constructs with spatial control over cellular distribution but often solvents employed in the spinning process are problematic due to their high cytotoxicity. Herein, microfluidic cell encapsulation is used to establish a temporary protection vehicle for the *in situ* delivery of cells for the development of a fibrous, cell-laden hybrid biograft. Therefore a layer-by-layer process is used by alternating fiber electrospinning and cell spraying procedures.

Both encapsulation and subsequent electrospraying of capsules has no negative effect on the viability and myogenic differentiation of murine myoblast cells. Propidium iodide positive stained cells were analyzed to quantify the amount of dead cells and the presence of myosin heavy chain positive cells after the processes was shown. Furthermore, encapsulation successfully protects cells from cytotoxic solvents (such as dimethylformamide) during *in situ* delivery of the cells into electrospun poly(vinylidene fluoride-co-hexafluoropropylene) scaffolds. The resulting cell-populated biografts demonstrate the clear potential of this approach in the creation of viable tissue engineering constructs.

Statement of Significance

Infiltration of cells and their controlled spatial distribution within fibrous electrospun membranes is a challenging task but allows for the development of functional highly organized 3D hybrid tissues. Combining polymer electrospinning and cell electrospraying in a layer-by-layer approach is expected to overcome current limitations of reduced cell infiltration after traditional static seeding. However, organic solvents, used during the electrospinning process, impede often major issues due to their high cytotoxicity. Utilizing microfluidic encapsulation as a mean to embed cells within a protective polymer casing enables the controlled deposition of viable cells without interfering with the cellular phenotype. The presented techniques allow for novel cell manipulation approaches being significant for enhanced 3D tissue engineering based on its versatility in terms of material and cell selection.

1. Introduction

In the field of tissue engineering, the development of artificial functional tissues is largely controlled by cell culture substrates that provide the tissue with specific biological, chemical, architectural and mechanical properties and cues. Despite a continual development of new manufacturing techniques that allow the engineering of 3D scaffolds, the ability to mimic native tissues in an efficient and reproducible manner remains a complex challenge.

* Corresponding author.
E-mail addresses: lukas.weidenbacher@empa.ch (L. Weidenbacher), afshin.abrishamkar@chem.ethz.ch (A. Abrishamkar), markus.rottmar@empa.ch (M. Rottmar), geraldine.guex@empa.ch (A.G. Guex), katharina.maniura@empa.ch (K. Maniura-Weber), andrew.demello@chem.ethz.ch (A.J. deMello), sferguson@ethz.ch (S.J. Ferguson), Rene.Rossi@empa.ch (R.M. Rossi), giuseppino.fortunato@empa.ch (G. Fortunato).
[1] These authors contributed equally.

https://doi.org/10.1016/j.actbio.2017.10.012
1742-7061/

In the human body, tissues are composed of spatially distributed cells within a tissue-specific extracellular surrounding made of various components [1,2]. To mimic such a sophisticated environment using engineering approaches, not only the material choice and scaffold morphology need to be considered, but also the incorporation and subsequent interaction of host cells (which determine cell fate) within the construct [3]. While parameters such as average pore size and overall scaffold porosity are known to be of key importance for maintaining cellular function [4–7], cellular infiltration of a 3D scaffold and the formation of a multilayer, truly 3-dimensional tissue still remain a significant challenge.

Another prerequisite aside the scaffold architecture is the mechanical support, which should resemble the native tissue environment and can also be considered as a general requirement [9]. This feature is limiting the usage of natural polymers for tissue engineered scaffolds since their mechanical support is too low. To adjust mechanical properties in a controlled manner, polymer blending [10] or crosslinking with potentially cytotoxic crosslinking agents or photoinitiators [11,12] is necessary. As a consequence, mostly synthetic polymers with superior intrinsic mechanical features (such as flexibility or modulus) are used for tissues for which adapted mechanical support is a prerequisite [13,14]. Stable polymers are applied *in vivo* for vascular and cardio-vascular intervention as vascular graft materials [15] or engineering of tri-leaflet heart valves [16]. They are also being investigated for treatments of the spine [17] or ligament [18]. Besides these, they are commonly applied in designing advanced anti-adhesive or functional *ex vivo* wound dressings [19].

Furthermore, synthetic polymers are particularly attractive in terms of manufacturing standardization as well as off-the shelf availability when it comes to clinical requirements [2].

Amongst these, poly(vinylidene fluoride-co-hexafluoropropy lene) (PVDFhfp) is a highly fluorinated synthetic polymer with the potential for long term *in vivo* applications. Due to its chemical structure, it is highly resistant to hydrolytic, oxidative and enzymatic cleavage [20]. In addition, since fluorinated surfaces have been shown to enhance thromboresistance [21,22], PVDFhfp is a promising material for blood contact applications. It can also be exploited in the design of scaffolds in neuronal, cardiac or skeletal muscle tissue where electrical stimulation is beneficial [23]. Indeed, it has been found that electric stimuli can promote the differentiation of murine myoblast cells into functional contractile myofibrils, needed for engineering functional skeletal muscle tissue [24,25].

A combination of electrospinning and cell electrospraying showed much promise for the incorporation of cells into three-dimensional fibrous scaffolds [26,27]. Importantly, such an approach could be exploited to avoid post-seeding strategies, where seeding densities and cellular distribution are difficult to control [28].

However, in most electrospinning processes, synthetic polymers must be first dissolved in cytotoxic organic solvents [29], thus limiting their utility in cell-based applications. Whilst electrospinning from benign solvents has been investigated [8,30], its use has been limited to water soluble polymers, which in turn promotes rapid scaffold dissolution in the aqueous cell culture environment.

To overcome the issue of solvent toxicity, it has been suggested that cells should be "protected" during the manufacturing process [26], since simple post-processing methods allow the removal of residual solvents [29].

Indeed, encapsulating cells in alginate, collagen or agarose [31], affords not only some degree of environmental protection but also a controlled release of cells [32]. Such "microcarriers" have been widely investigated as potential delivery vehicles in therapeutic applications such as the treatment of myocardial diseases [33]. Moreover, since the transport of cytokines and other molecules from such capsules to the surrounding tissue can occur with ease, there is much potential for application in cell-based therapies [34,35]. Conversely, it must also be remembered that capsules can inhibit or delay a host immune response by blocking immune cell recognition sites [36].

In recent years, microfluidic technologies have been used to excellent effect in a range of biological applications such as synthesis of functional materials, drug discovery and single cell studies [37–39]. In relation to the current studies, microfluidic tools have been shown to be especially useful in generating monodisperse capsules for single cell entrapment [40,41] as well as in the controlled release of cells [32]. Additionally, the combination of microfluidics with electrospinning and electrospraying has been shown to be a promising platform for a range of operations in cell biology and tissue engineering [42,43].

Herein, we describe how the use of electrohydrodynamic and microfluidic technologies can be applied to create a droplet-based microfluidic platform integrated with electrospraying/electrospinning for the fabrication of hybrid membranes composed of a synthetic polymer and living cells. Specifically, we leverage controlled droplet formation at a flow-focusing geometry to encapsulate cells in gelatin microcapsules for the generation of protective transport vehicles. Subsequent electrospraying of these carriers coupled with electrospinning of polymeric fibers is then demonstrated. Finally, we assess the effect of these processing steps on the viability and differentiation of C2C12 myoblast cells and the resulting hybrid constructs via flow cytometry of propidium iodide stained cells and immunohistochemistry staining for myosin heavy chain.

2. Materials and methods

2.1. Materials and reagents

All materials were purchased from Sigma Aldrich (Buchs, Switzerland), unless otherwise noted. All materials were used as received and without any further purification. Cell culture supplements and reagents were from Thermo Fisher Scientific (Waltham, USA) and used as received.

2.2. Cell culture

All *in vitro* experiments were performed using a murine skeletal myoblast cell line (C2C12, ATCC, Manassas, USA) at passage 13–16. Cells were expanded/cultivated in Dulbecco's modified Eagle Medium (DMEM) supplemented with 10% fetal calf serum (FCS) and 1% penicillin (5 mg ml^{-1})/streptomycin (5 mg ml^{-1})/neomycin (10 mg ml^{-1}) incubated in a humidified environment at 37 °C and 5% CO_2. When 90% confluency was reached, cells were harvested and suspended in 5% w/v gelatin (dissolved at 37 °C in DMEM) derived from porcine skin in a 50 ml falcon tube (Corning, New York, USA). The solution was vortexed (Vortex Genie 2, Scientific Industries, New York, USA) and kept in a water bath at 37 °C until further use. All experiments were performed at a total concentration of 3×10^6 cells ml^{-1}.

2.3. Microfluidic device fabrication

Microfluidic devices were fabricated by replica molding of PDMS (SYLGARD 184 Silicone Elastomer Kit, Dow Corning®, USA) against a structured silicon master mold, previously fabricated using standard photolithographic methods, and described in detail elsewhere [44]. Briefly, a mixture of PDMS elastomer and curing agent at a 10:0.9 w/w ratio was poured over the master (previously

treated with chlorotrimethylsilane) and cured in an oven at 70 °C for two hours. The cured PDMS molds were then cut into rectangles (45 mm × 25 mm) using a razor blade, with 1 mm diameter inlet and outlet holes formed using biopsy punches. Finally, PDMS molds were bonded to glass coverslips (76 mm × 26 mm, Thermo Fisher Scientific, Waltham, USA) after plasma activation of both the glass and PDMS surfaces under corona discharge (Electro-Technic Products, USA; power input of 30 W at 4.5 MHz). The microfluidic device contains three inlets (two for continuous phase and one for dispersed phase) and one outlet. Integrated microchannels had widths ranging between 40 and 200 μm and a height of 45 μm. A schematic of the microfluidic design is presented in Fig. 1a.

2.4. Microcapsules formation and cell encapsulation

A cell-laden gelatin solution (3×10^6 cells ml^{-1}) and a carrier fluid consisting of light mineral oil (density: 0.838 g ml^{-1} at 25 °C) with 0.25% Span-80 were used to form microcapsules. A secondary oil flow (containing light mineral oil with 3% Span-80) was used downstream of the droplet generation region to control the segmented flow and enhance the formation of monodisperse microcapsules. Fluids were delivered to the inlets of the microfluidic device using a syringe pump system (neMESYS module, Cetoni GmbH, Germany), with the flow rates set to 5 μl min^{-1} and 30 μl min^{-1} for the gelatin and oil flows, respectively [45]. The gelatin and oil flows are segmented at the flow focusing droplet

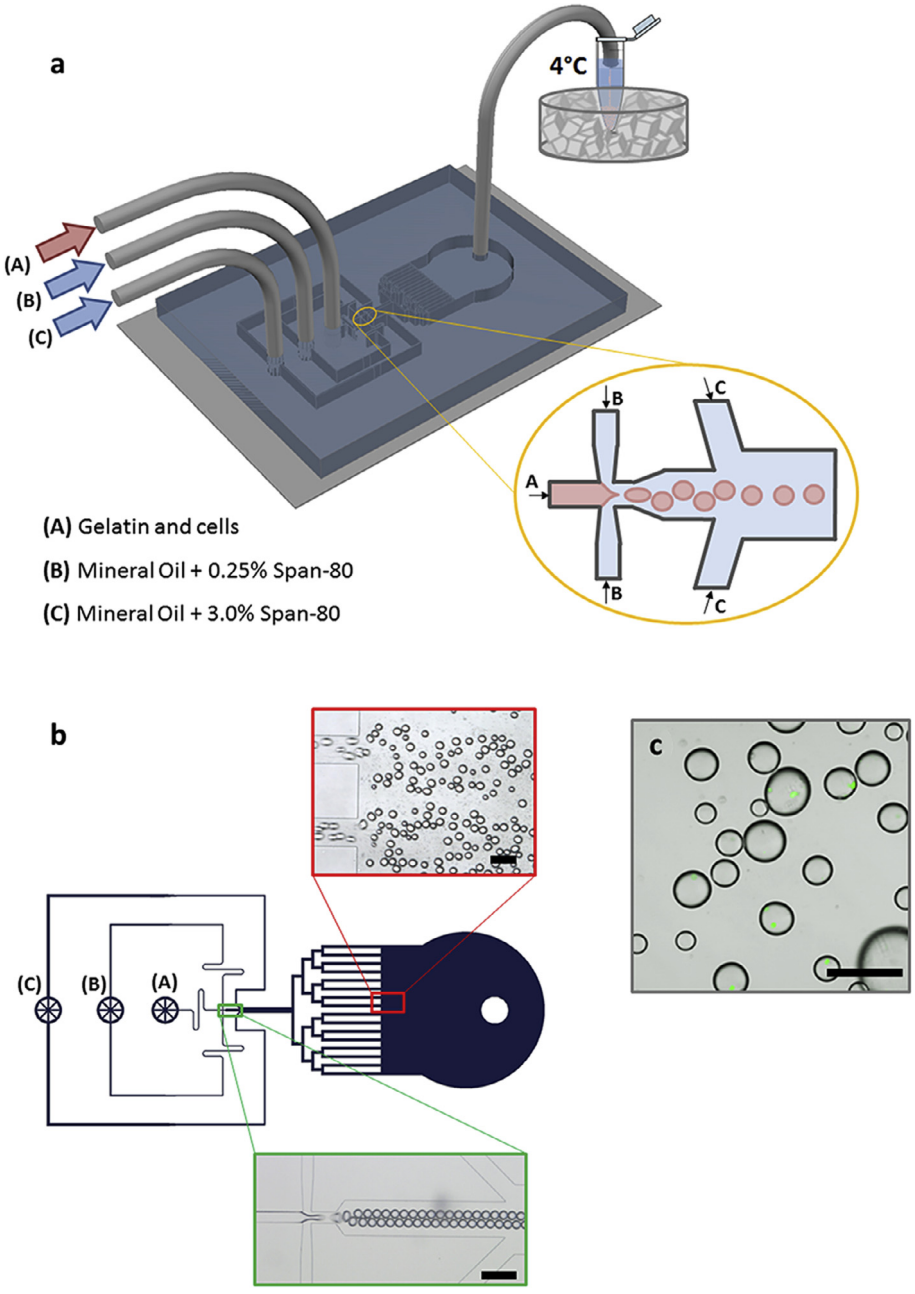

Fig. 1. (a) Schematic illustration of the microfluidic device and the encapsulation process including the collection of the generated microcapsules in an ice bath. The inlay schematically illustrates the droplet generation region. (b) The design of the microfluidic device, with the optical micrographs of its different sections during the process. (c) Microcapsules collected in oil with cells stained with a live dye showing the result of the encapsulation process. Scale bars: 200 μm.

geometry to form microcapsules. The microcapsules are then driven through an expansion zone where the channel width expands from 60 to 200 μm over the length of 50 μm, enhancing the formation of stable microcapsules. Downstream, a secondary flow of oil (with higher surfactant concentration) is introduced at a flow rate of 35 μl min^{-1}. The generated microcapsules then pass through a bifurcation region comprised of 16 parallel (200 μm wide) microchannels, which further stabilize the microcapsules, before exiting the microfluidic device. The microcapsules were collected directly from the outlet into a 1 ml Eppendorf tube (Eppendorf, Switzerland), submerged in an ice bath, and allowed to settle. The microfluidic encapsulation process via microfluidics was run for 1.5 h before the subsequent oil extraction step.

2.5. Capsule separation

Excess oil was removed with a pipette before the extraction. The remaining liquid was then put on an electrospun PVDFhfp membrane (Mw: 400,000 Da, prepared as described in section 2.10). This allowed removal of any excess oil, leaving the microcapsules on the surface. These were then flushed into a petri dish with 200 μl of cold (4 °C) cell culture medium. The process was repeated until the oil phase was fully adsorbed into the PVDFhfp membrane, with extracted capsules being stored in DMEM in an Eppendorf tube on ice.

2.6. Capsule characterization

Images of the capsules after the different production steps were taken using an optical microscope (Primovert equipped with an Axiocam 105 color, Zeiss, Oberkochen, Germany). The diameters of the capsules were measured using Image J [46]. The average diameter of a total of 200 capsules was taken from three individual experiments. To determine the number of cells per capsule, 10 images (1141 capsules in total) from three individual experiments were analyzed and cell numbers manually counted. Additionally, we adopted a protocol described by Mazutis et al. to estimate the number of cells encapsulated per capsule assuming Poissonian distribution [47], Eq. (1):

$$P_x = \frac{e^{-\lambda} * \lambda^x}{x!} \quad (1)$$

where P represents the probability of x cells per capsule and λ represents the mean number of cells per capsule calculated with the experimental parameters (by use of the initial cell concentration and the average capsule volume, x = number of cells).

2.7. Spraying of capsules and cell release

Capsules were sprayed in cell culture medium. A conventional electrospraying setup described elsewhere [48], modified for a vertical setup was used for all experiments. Briefly, 200 μl of capsules in DMEM, purified from the light mineral oil as described in section 2.4, were placed in a 1 ml syringe tipped with a blunt 21G stainless steel needle (B. Braun, Melsungen, Germany). A positive voltage of +9 kV was applied to the needle. A petri dish containing 500 μl of cell culture medium was placed at 5 cm distance to the needle to collect the capsules. The petri dish was placed on a metal plate where a negative bias of −3 kV was applied to direct the capsules into the dish.

Cell release from gelatin capsules was monitored using a confocal laser scanning microscope (CLSM, LSM 780, Zeiss, Germany). For live imaging, cells were stained with the lipophilic tracer DiD (20 μg ml^{-1}). Gelatin from porcine skin, labelled with Oregon Green® was added to the gelatin used for the encapsulation at a ratio 1:1000 v/v. To induce gelatin dissolution and the release of the cells the temperature was increased to 37 °C.

2.8. Cell viability

A LIVE/DEAD® staining kit for mammalian cells (Thermo Fisher Scientific, Waltham, USA) was used to stain living cells green (calcein AM, 4 mM in anhydrous DMSO, 1:2000) and dead cells red (ethidium homodimer, 2 mM in DMSO/H_2O 1:4 v/v, 1:2000). The staining was performed in DMEM cell culture medium instead of PBS. Other than that the protocol of the manufacturer was followed. Images were taken after 24 h under cell culture conditions (37 °C, 5% CO_2). Cells were stained for 10 min in DMEM prior to imaging. During this period cells were released from the gelatin microgel due to gelatin dissolution. Cells cultivated on tissue culture polystyrene TCPS (Corning, New York, USA) were used as positive controls and cells treated with 0.2% digitonin (Sigma Aldrich, Switzerland) in DMEM for 5 min at 37 °C as negative controls. For quantitative analysis of viable cells, a propidium iodide stain was used and measured by flow cytometry (Gallios, Beckman Coulter, Germany) (n = 3 individual experiments). Capsules were kept in an incubator in an Eppendorf tube until the gelatin was fully dissolved. Subsequently, cells were centrifuged and stained for 15 min on ice. Staining solutions were prepared using a binding buffer (1x Annexin V Binding Buffer, BD Biosciences, Switzerland) and propidium iodide at the ratio 9:1 v/v. Living cells and dead cells were used as positive and negative control, respectively. For the negative control, cells were heated to 57 °C for 20 min to induce necrosis. The final percentage of dead cells was recorded by gating for higher signals of propidium iodide.

2.9. Cell characterization

After oil removal and spraying of the capsules, cells were cultivated until confluency was reached (approximately 4–5 days). Myotube formation of C2C12 cells was induced by change to serum deprived medium (DMEM supplemented with 1% horse serum (Gibco, Invitrogen, USA) and 1% PSN). Medium was changed every other day for a differentiation period of 7 days. Cells were stained for immunohistochemistry with fluorescent dyes for the nuclei (1:1000, DAPI) and actin (1:40, Alexa Fluor® 488 or 647 Phalloidin, Thermo Fisher Scientific). Differentiated cells were stained for myosin heavy chain (1:400, Sigma Aldrich, Switzerland) conjugated to a fluorescently labelled secondary antibody (1:400, Goat anti mouse IgG, Alexa Fluor® 488, Thermo Fisher Scientific). Prior to staining, samples were blocked (5% goat serum, 1% FCS in PBS). Staining was performed in PBS supplemented with 1.5% w/v skimmed milk (Rapilait, Migros, Switzerland). All experiments were repeated at least 3 times.

To observe incorporation of cells into the electrospun membrane, scanning electron microscopy was performed with an acceleration voltage of 2 kV and 10 mA current flow (Hitachi S-4800, Hitachi High-Technologies, US, Illinois, USA). Prior to imaging, samples were fixed in modified Karnovsky solution (4% paraformaldehyde, 2.5% glutaraldehyde) for 1 h and dehydrated in an ascending ethanol series from 50% to 100% (30–60 min incubation for each concentration) and finally dried in hexamethyldisiloxane for 5 min.

2.10. Analysis of residual solvent in electrospun membranes

The presence of residual N,N-dimethylformamide (DMF) (boiling point 153 °C) in the membranes was measured via gas chromatography-mass spectroscopy (Head space GC–MS). An Agilent G1530A gas chromatograph coupled with an HP 5973 mass spectrometer was used for all experiments. Thereby, the sample

was heated starting from a temperature of 50 °C (held for 1 min), which was ramped up to 250 °C at a rate of 15 °C min^{-1}, where the temperature was held for 1 min. Eluents were collected on a solid phase microextraction fiber (SPME Fiber 65 μm PDMS/DVB fused silica 24 Ga for use with manual holder, Sigma Aldrich, Switzerland) and separations performed on a HP-5MS GC column (Agilent technologies, USA) (30 min at room temperature).

2.11. Electrospinning/capsule spraying

The experiments were not performed under sterile conditions. However the device as well as the instruments were thoroughly cleaned with 70% ethanol beforehand. Parameters for cell spraying were as described previously. For electrospinning, PVDFhfp was dissolved in DMF at a concentration of 35% w/v. A planar stainless steel plate collector was placed at a distance of 20 cm from a syringe filled with the polymer solution. The polymer solution was ejected at a flow rate of 20 μl min^{-1} using a syringe pump (World Precision Instruments, Sarasota, USA, model: Aladin 1000). To characterize the intrinsic pore size of the polymeric membrane, capillary flow porometry was used (POROLUX™ 1000, POROMETER nv, Belgium). The cell-laden membrane was fabricated in a layer-by-layer approach. After 60 min of electrospinning, capsules were sprayed on top of the membrane at a flow rate of 50 μl min^{-1}. In order to spray the required amount of cells in a volume of 200 μl, the spraying duration was 4 min. Subsequently a layer of PVDFhfp was spun for 5 min on top of the capsules. To remove residual solvent, the biograft was then washed with cold PBS (4°C) for 60 min in a cell culture dish, with the PBS being changed every 10 min. After washing the membrane was cultivated under culture conditions in cell culture medium. To validate the reproducibility of this approach, the experiment was repeated three times.

2.12. Statistical analysis

Pearson correlation coefficient (r^2) was calculated between the frequency distributions of predicted values from Eq. (1) and experimental data (n = 3) of encapsulated cells per capsule. An unpaired two-tailed Student's *t*-test was used to determine significance. Differences with p-value < 0.05 were considered statistically significant. Statistical analyses were performed in Graphpad Prism 7.

3. Results

3.1. Cell encapsulation

The microfluidic device used herein is designed to generate stable gelatin-in-oil microcapsules, with diameters between 40 and 140 μm, at a rate of 150–200 per second [45]. Cell-laden gelatin and oil flows were injected at 5 μl min^{-1} and 30 μlmin^{-1}, respectively, leading to formation of microcapsules with an average diameter of 112 μm ± 30 μm (Fig. 1). To overcome potential backpressure issues, which occur in long microchannels and can cause failure of the chip, flow rates were optimized as previously described [49]. Microcapsules passed through a short expansion zone where they were stabilized due to shear. Downstream a second flow of continuous phase was introduced from both sides at a flow rate of 35 μl min^{-1}. This auxiliary flow of continuous phase guides the flow of generated microcapsules to the centerline of the channel, improving the monodispersity of the microcapsules and suppresses the jetting along the channel.

3.2. Capsule purification and processing

The different process steps for capsule purification are shown in Fig. 2. After the purification the capsules were sprayed into a cell culture dish filled with cell culture medium. Significantly, and as shown in Fig. 3a and b, electrospraying had no influence on the morphology of the formed capsules. All capsules remained intact without any major deformation or swelling, with an average diameter of 112 μm ± 30 μm (114 μm ± 31 before spraying, 110 μm ± 29 μm after spraying). Within the measured capsules (n = 1141), a total number of 1729 cells were successfully encapsulated with 66% of the capsules being laden with cells (Fig. 3c). A good agreement ($r^2 = 0.984$, $p = 3.3 \cdot 10^{-11}$) was found between estimated values (from Eq. (1)) and experimental data (Fig. 3c).

3.3. Cell characterization

LIVE/DEAD staining results, both after capsule extraction and after spraying, are presented in Fig. 4(a, d and g). Fluorescence images confirm that cell viability was not significantly impaired after each processing step when compared to the positive control. This is further supported by flow cytometry data (Fig. 4c, f and i) with 84%, 82% and 81% (n = 3) of the cells being viable in the control group, after the oil removal and after the capsules have been sprayed by the electrostatic field, respectively (measured by counting PI positive cells). The scatterplots shown in Fig. 4b, e and h, allow identification of viable and dead populations, as dead cells reveal lower forward scatter signals and higher side scatter signals. Interestingly, discrimination was less obvious for the control group.

After cultivating the cells in differentiation medium for 7 days, the impact of the process steps on differentiation potential (into multinucleated myotubes) was assessed.

Fig. 5a depicts differentiated cells after oil removal. By staining for actin and cell nuclei it can be seen that single cells merged and formed elongated myotubes, as expected for C2C12 myoblasts. No differences were observed compared to both experimental groups (Fig. 5b and c). Additionally, all groups investigated were positive for the specific myosin heavy chain marker (Fig. 5d–f).

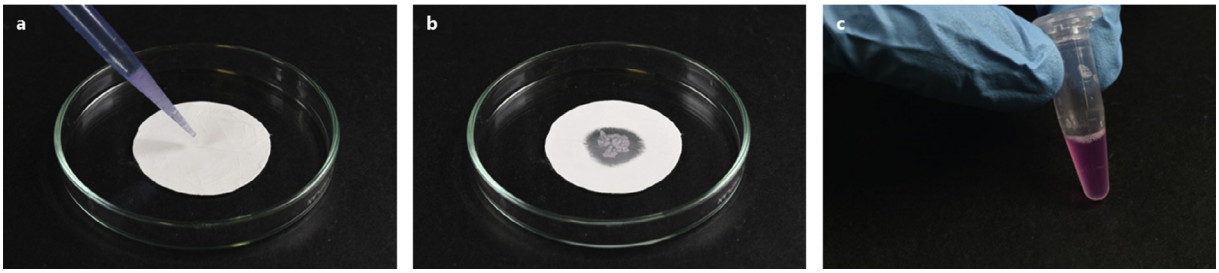

Fig. 2. Purification of the microgel capsules from the oil phase. (a) The oil containing the capsules is added onto the hydrophobic membrane. (b) After 1–2 min the oil was completely absorbed by the membrane. (c) The capsules were flushed with 200 μl of DMEM and stored in an Eppendorf vial on ice.

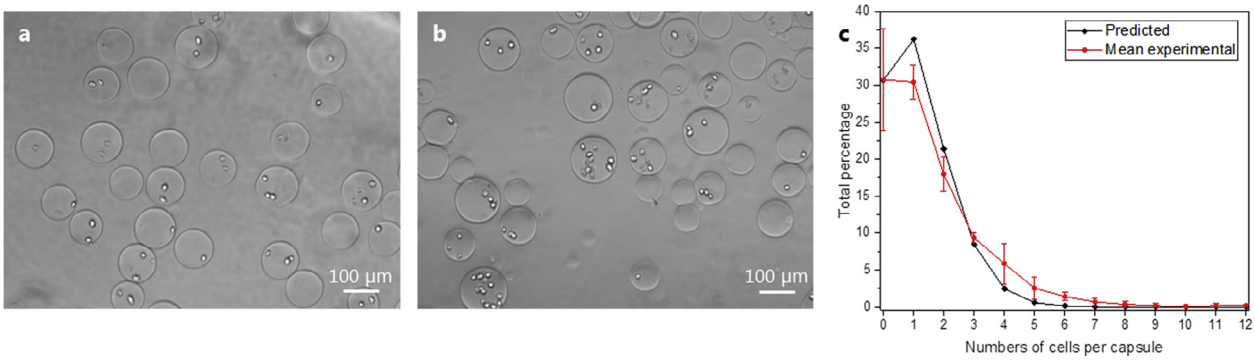

Fig. 3. (a) Collected capsules after the oil extraction on a PVDFhfp membrane and resuspension in cell culture medium. (b) The shape and size of capsules are maintained after spraying capsules from a 21G needle into a petri dish filled with cold cell culture medium, with an average capsule size of 112 µm ± 30 µm. (c) Comparison between experimental data and prediction model (based on Poissonian distribution) for the encapsulation process. Data represents mean ± SD of n = 3 independent repetitions in the experimental group and predicted values from Eq. (1).

3.4. Cell release from microcapsules

Cell release from capsules is shown in Fig. 6. Fluorescence images, taken after 1, 15 and 30 min, illustrate the dissolution of gelatin capsules over time at 37 °C with signal from the Oregon green labelled gelatin diminishing after 15 min due to water uptake. Complete dissolution of the gelatin occurs after approximately 30 min (Fig. 6c). The first signs of cell attachment to the dish can be observed by the formation of cellular protrusions that appear after capsules are fully dissolved, with the low intensity background signal resulting from dissolved fluorophore in the solution. Subsequent adhesion was also observed during LIVE/DEAD imaging experiments, with Calcein AM positive cells remaining attached and spread over the substrate 24 h after release (Fig. 4).

3.5. Hybrid biograft fabrication

The protective effect of the encapsulation was shown by the LIVE/DEAD staining of C2C12 cells after the combined process without encapsulation (Fig. 7b) as well as with encapsulation (Fig. 7c). Combined electrospinning of PVDFhfp and electrospraying of non-encapsulated cells was unsuccessful, since all cells were necrotic (Fig. 7b). Head-space GC–MS measurements indicated high amounts of "residual" DMF directly after electrospinning (Fig. 7a). While residues on the membranes were also measured after 2 h of storage in air, samples stored in PBS showed only a very small peak deriving from DMF.

Cell survival after the encapsulation process was significantly increased as demonstrated by the higher number of calcein AM positively stained cells (Fig. 7c). Cell proliferation within the biograft was reported by higher cell numbers on day 7 as seen in Fig. 7d. Living as well as dead cells were counted based on these images (n = 5 per group) revealing values of 0% (a), 77.75% ± 13.64% (b) and 87.08% ± 3.95%, respectively. We never experienced issues concerning contamination when the constructs were transferred into cell culture.

The presence of spread cells underneath the fiber layer was confirmed by SEM imaging of the construct produced by the described layer-by-layer process (Fig. 8a and b). This observation could be made in all the performed experiments (n = 3). Only small areas without cells were observed. Additionally, immunohistochemistry staining for actin and cell nuclei confirmed the cellular attachment to the scaffold (Fig. 8c).

4. Discussion

Production of scaffolds for *in situ* integration of cells to create functional 3D tissues is hampered by the usually required application of cytotoxic solvents or cross-linking agents [6,12]. Since fiber formation by electrospinning is highly dependent on the solvent system used (according to the used polymer), non-cytotoxicity cannot always be achieved as many synthetic polymers do not dissolve in e.g. aqueous solutions. For the reported polymer PVDFhfp, DMF is required to ensure spinning of homogenous fiber morphologies, and cytotoxicity of residual DMF within the fibers was observed after electrospinning (Fig. 7b). It is likely that the amount of remaining solvent in as-spun PVDFhfp is considerable due to a strong affinity of the solvent towards the polymer. DMF carrying a carbonyl group is able to form Lewis acid-base pairs with polymers like poly(vinylidene fluoride) [50], leading to semi-stable bonds with slow evaporation of the solvent. Similar interactions of polymers with solvents, e.g. hexafluoroisopropanol (HFIP) with polycaprolactone, were described by Nam et al. revealing solvent desorption over extended periods of time [29]. This affinity depends on the polymer-solvent combination as e.g. Stankus et al. did not observe any adverse effects with respect to cell survival when poly(ester urethane)urea was used with HFIP [26]. Furthermore, DMF has a relatively low vapor pressure implying slow diffusion kinetics compared to solvents with a high volatility like chloroform, THF or HFIP. In general it can be stated that solvents with a low vapor pressure remain longer in the fibers [51]. While washing the membranes for 2 h with water removed most of the remaining solvent (Fig. 7a), such an incubation step is not compatible with the approach of *in situ* integration of cells in the scaffold. Therefore, microfluidic cell encapsulation was utilized for the temporary protection of cells to maintain cell viability during the fabrication of hybrid biografts.

From the various techniques that have been described for the fabrication of microencapsulated cells [41,52], a microfluidic platform was selected due to the ease with which highly monodisperse microcapsules can be produced and because of the potential to control capsule size, throughput and encapsulation efficiency in a direct manner. The described microfluidic system allowed the preparation of microcapsules with an average diameter of 112 µm ± 30 µm. With the capsule size being a limiting factor for a successful electro-spraying process, this was well within the intended size range of <500 µm, being a limiting factor for a continuous electro-spraying process.

Establishing the optimal parameters for cell encapsulation, experimental parameters like flow rate, cell concentration as well as gelatin concentration were optimized, to achieve a stable process with low numbers of empty capsules. It was found that initial cell concentrations not only affected the efficiency of the process, but also the overall viscosity of the gelatin phase, which in turn influenced the performance of the microfluidic approach. Higher cell concentrations lead to faster gelation of the gelatin within

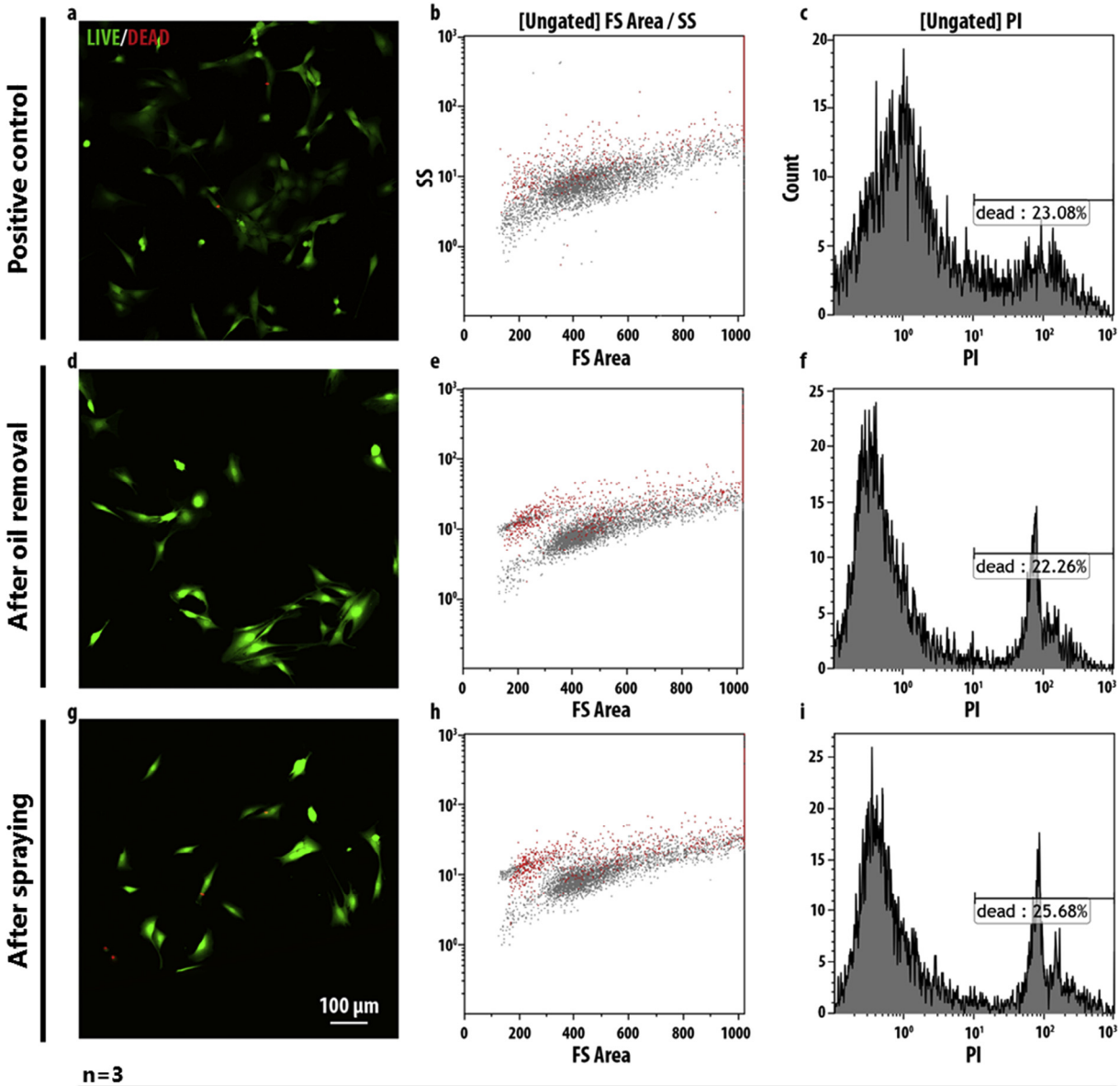

n=3

Sample name	Positive control	Negative control	After oil removal	After spraying
Total viability in %	83.96 ± 6.80	1.29 ± 0.95	81.87 ± 7.87	81.31 ± 6.64

Fig. 4. Viability of cells after different process steps. Cells were released from the gelatin capsules and attached to TCPS after a 24 h incubation period at 37 °C. Viability was measured via LIVE/DEAD staining as well as flow cytometry. Associated results for the different process steps can be seen: (d–f) after oil removal and resuspension in DMEM and (g–i) after spraying the capsules in DMEM with 9 kV into cell culture medium in a petri dish. (a–c) Untreated cells served as control.

the microfluidic channels and blockage of the tubing within a few minutes (data not shown). However, Clausell-Tormos et al. observed that as soon as the initial cell concentration drops below a certain number, the probability of encapsulating more than one cell decreases to values of $p \leq 7\%$ [53]. Therefore, cell densities were chosen to achieve single cell encapsulation resulting in 66% of the capsules carrying at least one cell. The efficiency of the cell encapsulation process was also modelled assuming Poissonian distribution and the predicted occupancies were in good agreement with experimental observations (Fig. 3c). Indeed, Mazutis et al. [47] previously utilized this model to obtain capsules with the majority of droplets containing one cell. The results in the present study highlight the versatility of the microfluidic cell encapsulation process and the potential to adapt the process to meet individual requirements.

After the microfluidic encapsulation a dispersion of cell-laden capsules in oil is obtained. Different methods such as centrifugation or dissolution of oil have been proposed to purify the microfluidic capsules [41,47]. However, either the dissolution of oil in hexadecane had a negative influence on the stability of the capsules, or the forces applied to the capsules during centrifugation initiated fusing of the gelatin micro-spheres (data not shown). A purification protocol using hydrophobic filtration paper has previously been used to remove the oil phase [54]. Adaption of this approach, by using electrospun nanofibrous PVDFhfp membranes (known for their high porosity, oleophilic properties and the potential to split oil from water for purification purposes [55]) allowed uptake of the oil within 2 min, so that capsules could be easily flushed from the membrane surface to the cell culture medium. Importantly, capsules were observed to maintain their shape and

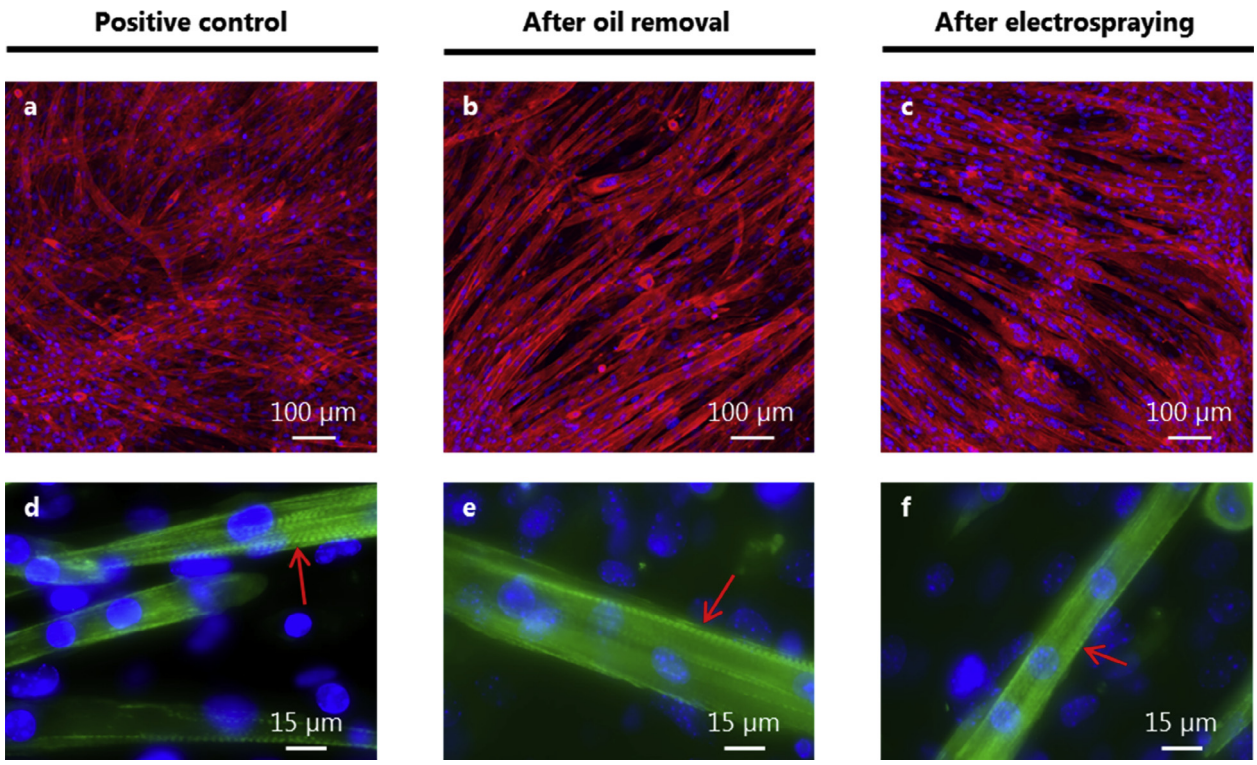

Fig. 5. Confocal laser scanning image of differentiated C2C12 cells (b) after encapsulation and removal of oil (c) as well as after the spraying process. (a) Untreated cells were used as control. Single cells merge to form typical bundle-like structured tubes. (d–f) All myotubes expressed myosin heavy chain as indicated by the red arrows.

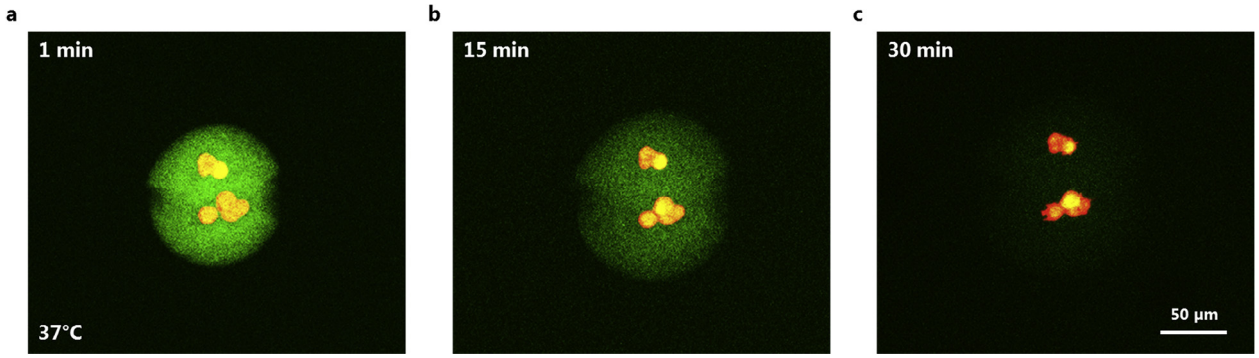

Fig. 6. Release of C2C12 cells from gelatin capsules monitored by time lapse imaging. After 30 min at 37 °C cells are released and start attaching onto the substrate. After 30 min, the first signs of cellular protrusions are visible, indicating the start of attachment to the underlying TCP substrate.

monodispersity throughout all the experimental steps including the subsequent electrospraying process where shear forces are applied, indicating sufficient mechanical stability of the capsules. One major advantage of gelatin was the possibility of triggering the cell release from the capsules in cell culture without the use of any additional treatments.

It has been previously reported that electrospraying of murine hematopoietic stem cells has no negative effect on either viability or phenotype [56]. Similarly, no changes of cell viability were observed for C2C12 cells within our study (Supplementary Fig. S1). In the current study, it was shown that both the cell encapsulation as well as the following electrospraying process do not negatively influence the behavior of myoblasts in terms of viability and myotube differentiation. Indeed, a total of 81 ± 6.6% of the cells were viable after the encapsulation, spraying and the release steps. In the control group 84 ± 6.8% of the cells were alive (Fig. 4). Additionally, cells were found to proliferate between day 1 and day 7 as observed by increasing cell numbers positively stained with calcein AM (Fig. 7c and d). As indicated by immunohistochemical analysis, characteristic differentiation of C2C12 cells into myotubes had occurred after culture in serum deprived media, with expression of myosin heavy chain being evident after 7 days (Fig. 5). Such phenotypical expression is in good agreement with results reported e.g. by Ricotti et al. with respect to the C2C12 behavior in terms of proliferation and differentiation when cultured on nanofiber membrane surfaces [57].

Furthermore, successful *in situ* integration of cells to create a hybrid biograft using a layer-by-layer approach based on electrospinning and electrospraying could be demonstrated (Fig. 8). SEM analysis showed the incorporation of cells in-between the spun layers without migration to the membrane surface due to the small mean pore size of 2.22 µm. This is an important finding since it demonstrates the possibility to spatially control the distribution of a cell population within a membrane. The electrospun layer seems to provide a barrier, mimicking natural barriers (such as the basement membrane found in blood vessel walls), where

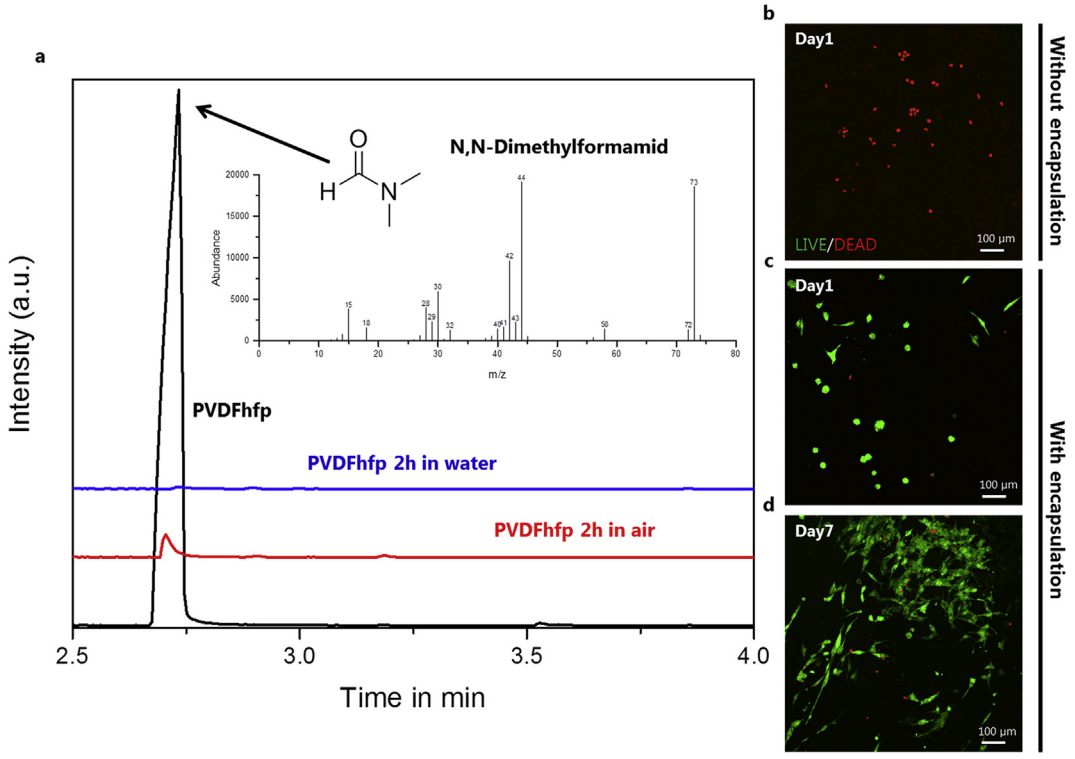

Fig. 7. (a) Mass spectra of electrospun membranes measured by GC–MS. The peak for residual DMF is depicted for the differently treated samples. LIVE/DEAD staining of C2C12 cells (b) sprayed into the membrane without encapsulation, (c) with encapsulation (d) as well as with encapsulation after 7 days in culture (n = 3).

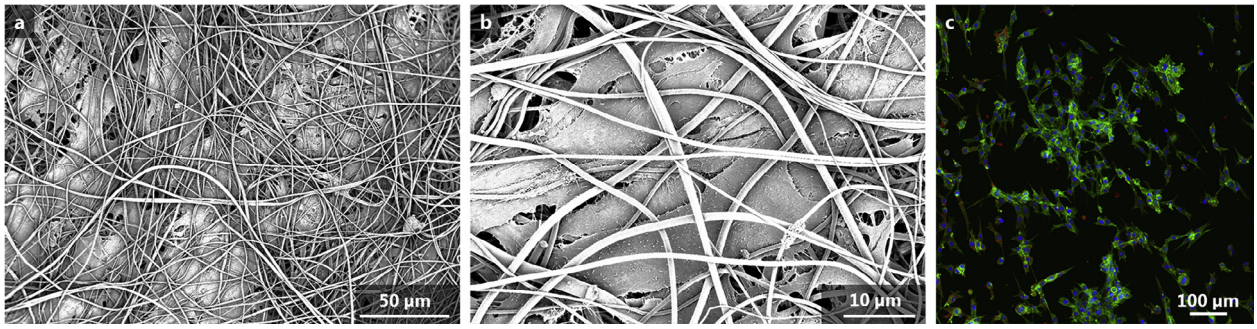

Fig. 8. (a and b) SEM micrographs of cells spread underneath a layer of electrospun fibers indicating the successful incorporation of C2C12 cells into the PVDFhfp scaffold. Images were taken after 7 days in culture. (c) The corresponding confocal laser scanning images confirm the presence of spread cells. Cells were stained for actin (green) and nuclei (blue).

spatial separation of different cell types is required. This is especially relevant for vascular applications, since smooth muscle cell proliferation and migration in the vascular system can cause pathological conditions such as intimal hyperplasia [58].

To further benefit from this potent combination of electrospinning and cell electrospraying, the experimental setup can be further developed to allow a simultaneous collection of fibers and encapsulated cells on a rotating drum. Overall, the presented approach suggests that complex functional tissues with spatially separated cells can be designed and fabricated.

5. Conclusion

The described method, which exploits microfluidic cell encapsulation and electrospraying/-spinning, provides a novel platform for controlled manipulation of cells and fabrication of hybrid biografts composed of viable cells and fibrous synthetic polymer scaffolds. Based on the protective effect of the microcapsules, cells are shielded from cytotoxic solvents utilized during electrospinning. Spraying cell-laden capsules does not affect viability or phenotype characteristics of the processed cells. Furthermore, the presented results provide a better understanding of solvent behavior during electrospinning. Finally, the presented approach has the potential to be adapted for different cell types and scaffold materials, and thus is likely to be a useful tool for targeted tissue reconstruction in applications such as vascular substitutes or other hierarchically structured 3D tissues.

Acknowledgements

The authors thank Dr. Mario Novkovic (Institute of Immunobiology, Kantonsspital St. Gallen) for the helpful assistance with the statistics. We are grateful to Elisabeth Michel (GC-MS measurements) and Dr. Nils Bohmer (FACS analysis) (Empa St. Gallen) for

their skillful help. This work is part of the Zurich Heart project of "Hochschulmedizin Zurich" (http://www.hochschulmedizin.uzh.ch/en/projekte/zurichheart.html).

Appendix A. Supplementary data

Supplementary data associated with this article can be found, in the online version, at https://doi.org/10.1016/j.actbio.2017.10.012.

References

[1] C.M. O'Connor, J.U. Adams, Essentials of Cell Biology, MA NPG Educ., Cambridge, 2010.
[2] F.J. O'Brien, Biomaterials & scaffolds for tissue engineering, Mater. Today 14 (2011) 88–95.
[3] L.G. Griffith, M.A. Swartz, Capturing complex 3D tissue physiology in vitro, Nat. Rev. 7 (2006) 211–224.
[4] H. Bergmeister, N. Seyidova, C. Schreiber, M. Strobl, C. Grasl, I. Walter, B. Messner, S. Baudis, S. Fröhlich, M. Marchetti-deschmann, M. Griesser, M. di Franko, M. Krssak, R. Liska, H. Schima, Biodegradable, thermoplastic polyurethane grafts for small diameter vascular replacements, Acta Biomater. 11 (2015) 104–113.
[5] A. Di Luca, K. Szlazak, I. Lorenzo-Moldero, C.A. Ghebes, A. Lepedda, W. Swieszkowski, C. Van Blitterswijk, L. Moroni, Influencing chondrogenic differentiation of human mesenchymal stromal cells in scaffolds displaying a structural gradient in pore size, Acta Biomater. 36 (2016) 210–219.
[6] T.A. Telemeco, C. Ayres, G.L. Bowlin, G.E. Wnek, E.D. Boland, N. Cohen, C.M. Baumgarten, J. Mathews, D.G. Simpson, Regulation of cellular infiltration into tissue engineering scaffolds composed of submicron diameter fibrils produced by electrospinning, Acta Biomater. 1 (2005) 377–385.
[7] Q. Liu, S. Tian, C. Zhao, X. Chen, I. Lei, Z. Wang, P.X. Ma, Porous nanofibrous poly (L-lactic acid) scaffolds supporting cardiovascular progenitor cells for cardiac tissue engineering, Acta Biomater. 26 (2015) 105–114.
[8] S. Das, F. Pati, Y.-J. Choi, G. Rijal, J.-H. Shim, S.W. Kim, A.R. Ray, D.-W. Cho, S. Ghosh, Bioprintable, cell-laden silk fibroin – gelatin hydrogel supporting multilineage differentiation of stem cells for fabrication of three-dimensional tissue constructs, Acta Biomater. 11 (2015) 233–246.
[9] S.J. Hollister, Porous scaffold design for tissue engineering, Nat. Mater. 4 (2005) 518–524.
[10] A. Sionkowska, Current research on the blends of natural and synthetic polymers as new biomaterials: review, Prog. Polym. Sci. 36 (2011) 1254–1276.
[11] K.T. Nguyen, J.L. West, Photopolymerizable hydrogels for tissue engineering applications, Biomaterials 23 (2002) 4307–4314.
[12] C.Z. Liu, Z.D. Xia, Z.W. Han, P.A. Hulley, J.T. Triffitt, J.T. Czernuszka, Novel 3D collagen scaffolds fabricated by indirect printing technique for tissue engineering, J. Biomed. Mater. Res. B Appl. Biomater. 85B (2008) 519–528.
[13] J.H. Park, J.M. Hong, Y.M. Ju, J.W. Jung, H.-W. Kang, S.J. Lee, J.J. Yoo, S.W. Kim, S. H. Kim, D.-W. Cho, A novel tissue-engineered trachea with a mechanical behavior similar to native trachea, Biomaterials 62 (2015) 106–115.
[14] S.C. Baker, G. Rohmann, J. Southgate, N.R. Cameron, The relationship between the mechanical properties and cell behaviour on PLGA and PCL scaffolds for bladder tissue engineering, Biomaterials 30 (2009) 1321–1328.
[15] R. Swathi, C.L. Elliot, Biomaterials for vascular tissue engineering, Regen. Med. 5 (2010) 1–21.
[16] D. Bezuidenhout, D.F. Williams, P. Zilla, Polymeric heart valves for surgical implantation, catheter-based technologies and heart assist devices, Biomaterials 36 (2015) 6–25.
[17] K.R.S. St John, The use of polyurethane materials in the surgery of the spine: a review, Spine J. 14 (2014) 3038–3047.
[18] C. Legnani, A. Ventura, C. Terzaghi, E. Borgo, W. Albisetti, Anterior cruciate ligament reconstruction with synthetic grafts. A review of literature, Int. Orthop. 34 (2010) 465–471.
[19] M.F. Maitz, Applications of synthetic polymers in clinical medicine, Biosurface Biotribol. 1 (2015) 161–176.
[20] N. Ding, S. Pacetti, F. Tang, M. Gada, W. Roorda, XIENCE V (TM) stent design and rationale, J. Interv. Cardiol. 22 (2009) S18–S27.
[21] T. Hasebe, S. Yohena, A. Kamijo, Y. Okazaki, A. Hotta, K. Takahashi, T. Suzuki, Fluorine doping into diamond-like carbon coatings inhibits protein adsorption and platelet activation, J. Biomed. Mater. Res. A 81 (2007) 1192–1199.
[22] X. Xie, R. Guidoin, M. Nutley, Z. Zhang, Fluoropassivation and gelatin sealing of polyester arterial prostheses to skip preclotting and constrain the chronic inflammatory response, J. Biomed. Mater. Res. B Appl. Biomater. 93B (2010) 497–509.
[23] R. Balint, N.J. Cassidy, S.H. Cartmell, Electrical stimulation: a novel tool for tissue engineering, Tissue Eng. Part B 19 (2013) 48–57.
[24] H. Park, R. Bhalla, R. Saigal, M. Radisic, N. Watson, R. Langer, G. Vunjak-Novakovic, Effects of electrical stimulation in C2C12 muscle constructs, J. Tissue Eng. Regen. Med. 2 (2009) 279–287.
[25] P.M. Martins, S. Ribeiro, C. Ribeiro, V. Sencadas, A.C. Gomes, F.M. Gama, S. Lanceron-Méndez, Effect of poling state and morphology of piezoelectric poly (vinylidene fluoride) membranes for skeletal muscle tissue engineering, RSC Adv. 3 (2013) 17938–17944.
[26] J.J. Stankus, J. Guan, K. Fujimoto, W.R. Wagner, Microintegrating smooth muscle cells into a biodegradable, elastomeric fiber matrix, Biomaterials 27 (2006) 735–744.
[27] J.J. Stankus, L. Soletti, K. Fujimoto, Y. Hong, D.A. Vorp, W.R. Wagner, Fabrication of cell microintegrated blood vessel constructs through electrohydrodynamic atomization, Biomaterials 28 (2007) 2738–2746.
[28] M. Chen, D.Q.S. Le, A. Baatrup, J.V. Nygaard, S. Hein, L. Bjerre, M. Kassem, X. Zou, C. Bünger, Self-assembled composite matrix in a hierarchical 3-D scaffold for bone tissue engineering, Acta Biomater. 7 (2011) 2244–2255.
[29] J. Nam, Y. Huang, S. Agarwal, J. Lannutti, Materials selection and residual solvent retention in biodegradable electrospun fibers, J. Appl. Polym. Sci. 107 (2008) 1547–1554.
[30] P.D. Dalton, K. Klinkhammer, J. Salber, D. Klee, M. Möller, Direct in vitro electrospinning with polymer melts, Biomacromolecules 7 (2006) 686–690.
[31] R.M. Hernández, G. Orive, A. Murua, J.L. Pedraz, Microcapsules and microcarriers for in situ cell delivery, Adv. Drug Deliv. Rev. 62 (2010) 711–730.
[32] D. Steinhilber, T. Rossow, S. Wedepohl, F. Paulus, S. Seiffert, R. Haag, A microgel construction kit for bioorthogonal encapsulation and pH-controlled release of living cells, Angew. Chem. Int. Ed. 52 (2013) 13538–13543.
[33] S. Zhao, Z. Xu, H. Wang, B.E. Reese, L.V. Gushchina, M. Jiang, P. Agarwal, J. Xu, M. Zhang, R. Shen, Z. Liu, N. Weisleder, X. He, Bioengineering of injectable encapsulated aggregates of pluripotent stem cells for therapy of myocardial infarction, Nat. Commun. 7 (2016) 1–12.
[34] T. Visted, T. Furmanek, P. Sakariassen, W.B. Foegler, K. Sim, H. Westphal, R. Bjerkvig, M. Lund-Johansen, Prospects for delivery of recombinant angiostatin by cell-encapsulation therapy, Hum. Gene Ther. 14 (2003) 1429–1440.
[35] H. Uludag, P. De Vos, P.A. Tresco, Technology of mammalian cell encapsulation, Adv. Drug Deliv. Rev. 42 (2000) 29–64.
[36] R. Krishnan, M. Alexander, L. Robles, C.E.F. Iii, J.R.T. Lakey, Islet and stem cell encapsulation for clinical transplantation, Rev. Diabet. Stud. 11 (2014) 84–101.
[37] A.B. Theberge, F. Courtois, Y. Schaerli, M. Fischlechner, C. Abell, F. Hollfelder, W.T.S. Huck, Microdroplets in microfluidics: an evolving platform for discoveries in chemistry and biology, Angew. Chem. Int. Ed. 49 (2010) 5846–5868.
[38] P.S. Dittrich, A. Manz, Lab-on-a-chip: microfluidics in drug discovery, Nat. Rev. Drug. Discov. 5 (2006) 210–218.
[39] D. Rodríguez-San-Miguel, A. Abrishamkar, J.A.R. Navarro, R. Rodriguez-Trujillo, D.B. Amabilino, R. Mas-ballesté, F. Zamora, J. Puigmartí-Luis, Crystalline fibres of a covalent organic framework through bottom-up microfluidic synthesis, Chem. Commun. 52 (2016) 9212–9215.
[40] E. Brouzes, M. Medkova, N. Savenelli, D. Marran, M. Twardowski, J.B. Hutchison, J.M. Rothberg, D.R. Link, N. Perrimon, M.L. Samuels, Droplet microfluidic technology for single-cell high-throughput screening, PNAS 106 (2009) 14195–14200.
[41] B.W. Tan, S. Takeuchi, Monodisperse alginate hydrogel microbeads for cell encapsulation, Adv. Mater. 19 (2007) 2696–2701.
[42] Y. Jun, E. Kang, S. Chae, S.-H. Lee, Microfluidic spinning of micro- and nano-scale fibers for tissue engineering, Lab Chip 14 (2014) 2146–2160.
[43] J. Hong, A.J. DeMello, S.N. Jayasinghe, Bio-electrospraying and droplet-based microfluidics: control of cell numbers within living residues, Biomed. Mater. 5 (2010) 1–6.
[44] A. Abrishamkar, M. Paradinas, E. Bailo, R. Rodriguez-trujillo, R. Pfattner, R.M. Rossi, C. Ocal, A.J. DeMello, D.B. Amabilino, J. Puigmartí-Luis, Microfluidic pneumatic cages: a novel approach for in-chip crystal trapping, manipulation and controlled chemical treatment, J. Vis. Exp. 113 (2016) 1–7.
[45] D.R. Griffin, W.M. Weaver, P.O. Scumpia, D. Di Carlo, T. Segura, Accelerated wound healing by injectable microporous gel scaffolds assembled from annealed building blocks, Nat. Mater. 14 (2015) 737–744.
[46] C.A. Schneider, W.S. Rasband, K.W. Eliceiri, NIH image to ImageJ: 25 years of image analysis, Nat. Methods 9 (2012) 671–675.
[47] L. Mazutis, J. Gilbert, W.L. Ung, D.A. Weitz, A.D. Griffiths, J.A. Heyman, Single-cell analysis and sorting using droplet-based microfluidics, Nat. Protoc. 8 (2013) 54–56.
[48] A.G. Guex, F.M. Kocher, G. Fortunato, E. Körner, D. Hegemann, T.P. Carrel, H.T. Tevaearai, M.N. Giraud, Fine-tuning of substrate architecture and surface chemistry promotes muscle tissue development, Acta Biomater. 8 (2012) 1481–1489.
[49] L. Mazutis, J. Baret, P. Treacy, Y. Skhiri, A.F. Araghi, M. Ryckelynck, V. Taly, A.D. Griffiths, Multi-step microfluidic droplet processing: kinetic analysis of an in vitro translated enzyme, Lab Chip 9 (2009) 2902–2908.
[50] Y. Ye, J. Rick, B. Hwang, Water soluble polymers as proton exchange membranes for fuel cells, Polymers (Basel) 4 (2012) 913–963.
[51] S. Kidoaki, I.K. Kwon, T. Matsuda, Structural features and mechanical properties of in situ-bonded meshes of segmented polyurethane electrospun from mixed solvents, J. Biomed. Mater. Res. Part B Appl. Biomater. 76B (2005) 219–229.
[52] C.J. Young, L.A. Poole-Warren, P.J. Martens, Combining submerged electrospray and UV photopolymerization for production of synthetic hydrogel microspheres for cell encapsulation, Biotechnol. Bioeng. 109 (2012) 1561–1570.
[53] J. Clausell-Tormos, D. Lieber, J.-C. Baret, A. El-Harrak, O.J. Miller, L. Frenz, J. Blouwolff, K.J. Humphry, S. Köster, H. Duan, C. Holtze, D.A. Weitz, A.D. Griffiths, C.A. Merten, Article Droplet-based microfluidic platforms for the encapsulation and screening of mammalian cells and multicellular organisms, Chem. Biol. 15 (2008) 427–437.
[54] D.-H. Lee, M. Jang, J.-K. Park, Rapid one-step purification of single-cells encapsulated in alginate microcapsules from oil to aqueous phase using a

hydrophobic filter paper: implications for single-cell experiments, Biotechnol. J. 9 (2014) 1233–1240.
[55] S.U. Patel, S.U. Patel, G.G. Chase, Electrospun superhydrophobic poly (vinylidene fluoride-co-hexafluoropropylene) fibrous membranes for the separation of dispersed water from ultralow sulfur diesel, Energy Fuels 27 (2013) 2458–2464.
[56] K. Bartolovic, N. Mongkoldhumrongkul, S.N. Waddington, S.N. Jayasinghe, S. J. Howe, The differentiation and engraftment potential of mouse hematopoietic stem cells is maintained after bio-electrospray, Analyst 135 (2010) 157–164.
[57] L. Ricotti, A. Polini, G.G. Genchi, G. Ciofani, D. Iandolo, H. Vazão, V. Mattoli, L. Ferreira, A. Meniciassi, D. Pisignano, Proliferation and skeletal myotube formation capability of C2C12 and H9c2 cells on isotropic and anisotropic electrospun nanofibrous PHB scaffolds, Biomed. Mater. 7 (2012) 2012.
[58] S.F. Louis, P. Zahradka, Vascular smooth muscle cell motility: from migration to invasion, Exp. Clin. Cardiol. 15 (2010) e75–e85.